Research Paper | Geology | E-ISSN : 2454-9916 | Volume : 1 | Issue : 5 | Dec 2015

DIAGNOSIS OF UPWELLING AND DOWNWELLING SIGNALS IN THE BAY OF BENGAL

Sourav Sil [1] | Arun Chakraborty [2]

[1] School of Earth, Ocean and Climate Sciences, Indian Institute of Technology Bhubaneswar, Bhubaneswar, Odisha, India

[2] Centre for Oceans, Rivers, Atmosphere and Land Sciences (CORAL), Indian Institute of Technology Kharagpur, Kharagpur, West Bengal, India

ABSTRACT

The monthly and interannual variations of upwelling and downwelling signal in the Bay of Bengal (BOB) have been investigated in this study using 52-years Simple Ocean Data Assimilation products (SODA). The intensity of upwelling and downwelling in the southern part is much higher than the other parts of BOB. The upwelling and downwelling in the BOB is not only driven by wind stress curl but also has significant contribution from the remote effect. The eastern coast and the central BOB are mostly dominated by remote effect. The wind-stress curl driven upwelling and downwelling in the open ocean is almost balanced by remote effect and as a result the central BOB does not show any upwelling and downwelling features during summer season. The increase of wind stress curl in the recent years over this region is another important outcome of this study. The Wind Stress Curl (WSC), vertical velocity and remote effect are influenced by the tropical climatic events like El-Niño/Southern Oscillation (ENSO) and Indian Ocean Dipole (IOD). The upwelling and downwelling signals became stronger during El-Niño and La-Niña years but during the concurrent ENSO and IOD years (1988 and 1997) this signals show different behavior for different boxes. There are quite similar responses of the BOB with El- Niño and positive IOD events and also with La- Niña and negative IOD events.

KEY WORDS: Bay of Bengal, Upwelling, Wind Stress, Remote effect

1. Introduction

The mechanism of oceanic upwelling and downwelling processes is very important to study as it affects the biological productivity and climate. It accounts for 80-90% of global ocean new productivity [Rao and Rama 2005]. During upwelling, the cold water comes from bottom to the surface with nutrients and chlorophyll and the warm water goes down during downwelling. Thus the distribution of heat flux is maintained in the vertical direction [Pond and Picard 2005].

The domain of our study is BOB which is located in the northeastern Indian Ocean (approximately 2°N - 22°N and 80°E - 100 E). It is a semi enclosed tropical ocean basin that is highly influenced by semiannually reversing wind. During winter monsoon, weak northeast winds bring cool and dry continental air to the BOB region, while, the strong southwest trade winds bring humid maritime air into the BOB region during the summer monsoon. The BOB receives large amount of fresh water from the river discharge [Subramanian 1993], as well as rainfall, mostly during the southwest monsoon that makes the upper layers water highly stratified with low salinity. The excess precipitation over evaporation [Prasad 1997] is prominent during this season. The BOB is also affected by severe tropical cyclones.

Several studies tried to understand the complex nature of the BOB and suggested the role of remote forcing in the semi-annual variability of the upper-layer circulation in the BOB [Potemra et al., 1991; Prasanna Kumar and Unnikrishnan 1995; McCreary et al., 1993, 1996; Shetye et al., 1996; Han and McCreary 2001; Han et al., 2001 and Somayajulu et al., 2003]. The remote forcing could arise by a variety of mechanisms, such as planetary waves originating at the eastern boundary excited by the energy radiated by the coastal Kelvin wave [Potemra et al., 1991; Yu et al., 1991; McCreary et al., 1993; Yu 2003, Paul et al., 2009], planetary waves generated by the variability in the local alongshore winds, and the interior Ekman pumping during the peak of summer and winter monsoons. It is natural to expect that these semi-annual atmospheric forcing as well as the remote forcing would modulate the thickness of the upper ocean by altering the thermal and mechanical inertia of the layer.

Shetye et al., [1991, 1993] based on hydrographic data and shipdrifts concluded that the BOB is driven mainly locally by wind stress curl but the role of remote driving proposed by Potemra et al., [1991] and McCreary et al., [1993] requires further investigation. Shankar et al., [1996] analyzed the dynamics of the East Indian Coastal Current (EICC) in the BOB forced by Ekman pumping confirmed the role of remote forcing. Another possible mechanism is coastal Kelvin waves propagating northward along the eastern boundary of the BOB excite westward propagating Rossby waves into the interior of the BOB [Yu et al., 1991; Yu 2003; Han and Webstar 2002 and Paul et al., 2009].

Several studies on the upwelling and downwelling over BOB basin were confined near the coastal region only [Suryanarayana and Rao 1993; Shetye et al., 1991, 1993]. There is no study available over the entire basin using the long time series oceanic dataset to investigate the mechanism of the above phenomena. Beside this, in recent years after the discovered of IOD [Saji et al., 1999] it has been reported by the researcher that the interannual variability of oceanic parameters in the equatorial Indian Ocean greatly influenced the circulations of the BOB and Arabian Sea [Somayajulu et al., 2003]. Jensen [2007] showed that the clockwise circulation in the Indian Ocean is intensified during El-Niño and IOD events and is weakened during La-Niña events. Fu [2007] showed that variability of Sea Surface Height is related to wind forcing at interseasonal frequencies.

In this paper we have studied the mechanism of upwelling and downwelling monthly and interannual signal using SODA dataset

and tried to identify the strong upwelling and downwelling zones over the BOB basin (Figure 1). The interannual variability of the upwelling and downwelling, WSC and remote effect signals and how they are influenced by the oceanic phenomena like El-Niño, La-Niña and IOD are also studied in this paper. We have also tried to find the dominant signals of the above parameters over the years.

2. Data and Methodology

In the present work, investigation is carried out to study the monthly and interannual variation of upwelling and downwelling signal in the BOB using the 52 years (1950 to 2001) global ocean monthly analysis datasets based on the SODA package of Carton et al., [2000a, 2000b]. This analysis uses a multivariate version of optimal interpolation in which the temperature, salinity and sea level fields are analyzed using statistical objective analysis. This is a well-known dataset as it has been used for the study of subsurface influence on Sea Surface Temperature (SST) [Rao and Behera, 2005] and Indian Ocean Dipole/Zonal Mode [Fischer et al., 2004] in tropical Indian Ocean region.

The Ekman transport may be calculated [Deser et al., 1999] by balancing the wind stress force with the Coriolis force due to ocean velocity (u and v) integrated over the Ekman layer as,

$$\left.\begin{aligned}\tau_x &= -\rho_0 f V_E \\ \tau_y &= \rho_0 f U_E\end{aligned}\right\} \quad (1)$$

where, ρ_0 is the density of seawater and f is Coriolis parameter. and are the wind stress components in zonal and meridional directions, and τ_x and τ_y are the wind stress components in zonal and meridional directions, and

$$\left.\begin{aligned}U_E &= \int_{z_E}^{0} u\,dz \\ V_E &= \int_{z_E}^{0} v\,dz\end{aligned}\right\} \quad (2)$$

where, z_E is the base of the Ekman layer.

Using the continuity equation again we can calculate the vertical motion (w_E) integrating the layer mean Ekman transports from the base of the Ekman layer as,

$$-\int_{z_E}^{0} \frac{\partial w}{\partial z} dz = \frac{\partial U_E}{\partial x} + \frac{\partial V_E}{\partial y}$$

$$\text{or, } w_E = \frac{\partial U_E}{\partial x} + \frac{\partial V_E}{\partial y} \quad (3)$$

Replacing the Ekman transport terms with the wind stress terms yields the relationship between Ekman pumping and the curl of the wind stress as,

$$w_E = \frac{\partial}{\partial x}\frac{\tau_y}{\rho_0 f} - \frac{\partial}{\partial y}\frac{\tau_x}{\rho_0 f} = \vec{k}.\vec{\nabla}\times\frac{\vec{\tau}}{\rho_0 f} \quad (4)$$

This Ekman pumping relation includes not only wind stress but also the beta effect.

In the Northern Hemisphere, positive wind stress curl causes divergence in the Ekman layer with upwelling (upward Ekman Pumping) but negative wind stress curl causes convergence in the Ekman layer with downwelling (downward Ekman pumping) and vice versa in the Southern Hemisphere [Pond and Picard, 2005].

The total vertical velocity is calculated diagnostically using continuity equation as,

$$w_{ver} = -\int (\frac{\partial u}{\partial x} + \frac{\partial v}{\partial y}) dz \quad (5)$$

where, u and v are the velocities along zonal and meridional directions respectively.

The remote component is obtained by taking the difference of the above two as,

$$w_{remote} = (w_{ver} w_E) \quad (6)$$

The advection term is calculated by using the following formula,

$$T_{ADV} = -(u\frac{\partial T}{\partial x} + v\frac{\partial T}{\partial y}) \quad (7)$$

Here according to our calculation the positive value of advection means that region gains heat and negative value of advection means losing heat.

3. Results and Discussions

3.1 Monthly Variability

The upwelling and downwelling of the BOB basin is influenced by the semi-annual reversing wind. So it is interesting to observe the monthly variation of upwelling and downwelling in that region. Here we have analyzed the monthly variations of WSC which indicates the converging or downwelling (negative value) and diverging or upwelling (positive value) zone. The vertical velocity is calculated at 37.5m depth in order to see the Ekman influence of this region. The positive value of vertical velocity means upwelling and negative value means downwelling. The monthly climatology of the above three parameters (w_{ver},w_E and w_{remote}) are calculated from 52 year dataset to study the variability.

3.1.1 Wind Stress Curl

The monthly climatology of WSC depicts the upwelling and downwelling regions over whole BOB (Figure 2). It indicates that there should be a downwelling zone in the western coast of the BOB (82˚E - 88˚E, 10˚N - 16˚N) during January to April. In the month of February, the intensity of wind stress curl attains its maximum value. Then the centre of this downwelling zone shifts towards the central BOB till the month of April. During these four months the WSC is almost negative all over the BOB. But from April, the upwelling is observed in the western coast of the BOB. During that time, negative WSC is observed in the eastern coast of the BOB (90˚E - 96˚E, 12˚N - 18˚N). This opposite characteristics may be due to the reversing wind over the BOB. During summer and late summer (May-September) the BOB divides into two parts (eastern and western) approximately around 90˚E, the upwelling in the western part and downwelling in the eastern part of BOB. The WSC is positive in the western side and negative in the eastern side. But in the late fall to early winter season (October-December), the WSC divides the BOB in north-eastern and south-western part with downwelling in the northern part and upwelling in southern part. It is also clear from the figure that the intensity of WSC is larger in the southern part of the BOB except in the winter and in the early spring season.

3.1.2 Vertical Velocity

The vertical velocity is calculated at 37.5m depth by using the equation (5) is shown in Figure 3. It shows that in the winter season i.e. from the month of December to February, strong downwelling in the north-western BOB. The similar pattern is also depicted in the Figure 2. During that time, north-easterly wind flows over BOB

and strong upwelling is observed in the eastern BOB. The north-eastward penetration of cold upwelled water from equatorial region around 85 E is evident during this time (Figure 4a). This is one of the evidence of remote effect to the BOB. It may be attributed to the meeting point of the reflected Kelvin wave from the western coast of the Indian Ocean basin and reflected Rossby waves from the eastern coast of Indian Ocean basin (Figure 4b) which is prominent in the month of April (Figure 3). In the summer when the south-westerly wind flows over the BOB region, the east and west BOB changes its nature. During that time, upwelling is observed in the west coast and downwelling in the east coast. As the wind is stronger than that of winter, the vertical velocity is larger in magnitude. During this time, the central BOB do not show any upwelling and downwelling features but the nature of the vertical velocity divides the BOB into two parts. This is due to the south-easterly wind flow and can be explained by similar mechanism as explained for the north-easterly wind during winter. This situation stays for the next few months from May to August. It becomes weak with time and in the month of September it is almost negligible. This may be due to the continuous rain during summer monsoon which makes the region highly stratified. The downwelling is observed at that location as northeast wind flows over BOB. The counter equatorial flow causes the downwelling feature in south of BOB during this time. The strong upwelling is observed from the month of May to October around Sri Lanka because of strong southwesterly wind. The magnitude of vertical velocity is almost same with WSC when EICC is not strong i.e. May to August [Shankar et al., 1996]. But except the above period, their magnitudes are different.

The role of horizontal advection to the vertical velocity can be seen from the temperature advection diagram (Figure 4c). It shows that from December to February there exists a warm water advection from the south into the BOB which helps to form a strong downwelling (Figure 3). During that time cold water advected to central BOB from eastern coast to the central BOB. As the time passes this cold water advection push back the warm water to the south and occupy most of the BOB during April although there is weak downwelling. During the month of May as the strong south west wind starts to flow over BOB, it reduces the cold water advection to the west, warm water starts to advect in the eastern BOB and cold water from the equator. During the month of July, cold water starts to penetrate from eastern coast of BOB to the central BOB region. During that time warm water advection takes place from the Arabian Sea to the BOB. In the summer, warm water advection from Arabian Sea is evident although there is strong upwelling in the eastern coast. In the month of September and October when the wind is changing its direction (from south westerly to north easterly), the warm water again starts to advect from the equator.

3.1.3 Remote effect

The Figure 5 shows the remote effect in different months over BOB. Figure 2 shows that there should be a strong downwelling in the northwest BOB during winter, but that is not reflected in Figure 3 indicating the existence of remote forcing by offshore or local wind stress curls [Shankar et al., 1996]. During that time WSC (Figure 2) shows converging or downwelling zone in the eastern BOB, but Figure 3 shows upwelling in that region. Therefore in winter, the remote effect from Malacca strait is prominent which is in favor of upwelling (Figure 5). In the summer, south-westerly wind (Figure 3) results downwelling in the east coast of BOB which is also seen in Figure 2. This indicates that remote effect is not prominent in this region in the summer. During that time upwelling occurs in the east coast line of India which can be seen both from vertical velocity and wind stress curl. During the month of May to November, value of remote effect shows negative value in southern BOB. It means remote effect is suppressing the influence of WSC. It can be concluded from the Figure 5 that the remote effect is not only confined in the eastern coast or around the Sri Lanka region but most of the BOB is dominated by remote effect throughout the entire year by the northward propagation of coastal Kelvin wave along the eastern coast of BOB and trapping of Kelvin and Rossby waves in the central part of BOB (between 10 N to 15 N) basin [Yu et al., 1991; Yu 2003; Han and Webstar 2002 and Paul et al., 2009]. During month of April to June, penetration of Kelvin wave through southern BOB and its spreading along the east coast of BOB are clear from Figure 5.

3.2 Interannual variability

The monthly variations of WSC, vertical velocity and remote effect are not uniform in different parts of BOB (Figures 2, 3, and 5). In order to study the interannual variability, four boxes (A, B, C, and D) have been chosen in this study.

a) Box-A: 81°E - 87°E, 13°N - 18°N
b) Box-B: 90°E - 96°E, 13°N - 18°N
c) Box-C: 81°E - 87°E, 5°N - 10°N
d) Box-D: 93°E - 99°E, 5°N - 10°N

These four boxes are very important as boxes A and B are directly linked with river discharge and semi-annual reversing winds, where box C is affected by penetration of Arabian Sea water flow as well as the equatorial effect ,and box D is directly affected by coastal Kelvin waves and penetration from Malacca strait. The interannual variability is shown for the variables used here in terms of indices [Chakraborty et al., 2006]. These indices were calculated from the monthly -climatology-removed anomalies of the time series data. The long-term time mean of the above anomalies was subtracted from each time series datum and normalized by dividing the standard deviation (s).

Previous studies suggested that on the interannual time scales the surface circulation of BOB is closely linked to the ENSO and its circulation responded to all the phases of ENSO events [Somayajulu et al., 2003]. We have tried to find the relation of the above parameters i.e. WSC, vertical velocity and remote effect with El-Niño and La-Niña years (Table 1) taken from www.cpc.noaa.gov. We have also performed wavelet analysis [Torrence and Compo 1998] to diagnosis the interannual signals.

3.2.1 Wind Stress Curl

Figure 6a represents that the interannual variability of wind stress curls in the southern part of the BOB are larger than the northern part (as value of standard deviation is larger). It is observed from this figure that before 1980 the interannual variations in all boxes are weak compared to the period after 1980 when variations increases in almost every box. In box A, there is sharp decrease in the interannual variations during 1990 to 1995 period but in box B, there is an increase of negative curl index during this period. In box C and D also, there are large variations. Overall analysis of this figure shows that the peak of the interannual signal, number of occurrences and many cases the duration in the BOB after 1995 for box A and after 1985 for other boxes increased. The changes of Sea Surface height and heat content in the oceans [Carton et al., 2005] and more frequent occurrence of strong equatorial climatic events after 1980 may be the cause of the above variations in the recent decades.

Wavelet analysis for WSC (Figure 6b) shows that there are many signals in the interannual variations almost for every box. For box A, no prominent signal is found before 1980, but after 1980 there is a 1-2 year signal in mid 1980s and 2-4 years signal in late 1990s. For box B, strong annual and semi-annual signal during 1964 and 1972 are found. There are also 1-2 year signal during 1988 and 1998. There are also 3-6 years signal in 1960s and 8 year signal in 1980s, but they are below 90 percent significant level. In case of box C, there is 2-6 years signal after 1980 and along with 1-2 year signal in late 1990s. For box D also there is a signal of 2-4 years in the late 1990s. Many of these prominent signals are associated with tropical climatic signals like ENSO and IOD. During strong El-Niño years the WSC is negative in southern BOB (box C and D)

resulting in downwelling and it is almost zero in upper BOB (box A and B) during those years except 1997-1998 which can be seen in Table 1. This exception may be due to overlapping of El-Niño and Indian Ocean Dipole (IOD) phenomena. During La-Niña years WSC is zero or positive in box A, C and D. But it is negative in 1975-1976 and 1988-1989 in box-B. The same features are also reflected from wavelet analysis (Figure 6b). During El-Niño the primary productions are very much less because downwelling increases but during La-Niña years the conditions are in favor of the primary productions due to increase of upwelling.

The impact of equatorial climatic signals to the variations of upwelling and downwelling during the winter months are evident from figure 9 (left column). It shows that WSC is lower in magnitude than climatology in both positive IOD and El-Niño events for almost all over the BOB. Southern BOB experience more downwelling in comparison to the northern side. But in the case of La-Niña event, WSC is larger in magnitude over climatology in the north-western BOB and the southern side of Sri Lanka, but lower in magnitude in the southern BOB. It is interesting to note that in the case of negative IOD event the signals are almost same like the La-Niña event and similar pattern is also observed by Jensen [2007] through the modeling study.

3.2.2 Vertical Velocity

The interannual variations of the anomalies in vertical velocity are shown in Figure 6a. The anomalies of vertical velocity in the box A and B (upper BOB) are lower than the other two regions as seen in case of WSC. In the same way, the variations increase after 1980 but not in large extent. In box D, from 1987 to 1996 there is continuous positive anomalies.

Wavelet analysis for vertical velocity (Figure 6b) shows the same indication like WSC. In box A, there are annual signal during 1955-1956, 1964-1965, 1988-1989 and 1997-1998. These are nothing but the El-Niño and La-Niña years. There are strong signals of 2-3 years during late 1960s and 1990s. In case of box B, there are strong signal during 1965, 1972, 1983 and in 1998. In that box wavelet spectrum shows that there is 4-6 years signal in 1965 and in 1980s, but the significance level is below 90 percent. In box C there are strong annual signal during 1977-1978, 1982-1983 and in the mid 1990s. This box shows a 3-6 years signal after 1980. In case of box D, there are same indications like the other boxes. During last 1960s and starting of 1970s a 2-4 years dominating signal is present. Table 1 shows that during strong El-Niño years, boxes A and B show positive value. But the boxes C and D show negative value except 1997. Again value of vertical velocity is zero and positive during the La-Niña years where in box A the value is negative except 1988-1989.

Figure 9 (middle column) shows that vertical velocity is larger in magnitude over climatology during El-Niño event case in the south-eastern side of the BOB and the southern side of Sri Lanka. The southern BOB experience downwelling feature during positive IOD year but the vertical velocity of the eastern BOB is larger in magnitude than the climatological value. In the positive IOD year Indonesian side of Indian Ocean experiences colder phase and as a result cold water enters the BOB to enhance the upwelling. But in the La-Niña year the picture is different from the above two cases. During that event, the vertical velocity is larger in magnitude in the south-eastern BOB and the southern side of Sri Lanka but smaller in area. The vertical velocity structure in the upper BOB during the negative IOD case is almost similar like the La-Niña event.

3.2.3 Remote effect

The interannual variations for the remote effect are shown in Figure 8a. The recent increase in variations like WSC and vertical velocity are not prominent for remote effect. The box A has less and box D has largest fluctuation. In box D, from 1987 to 1996 there is continuous positive anomalies in remote effect like vertical velocity. Therefore during this time remote effect is prominent in the Malacca strait region.

The Figure 8b shows that there are strong 2-3 years signal in box A during 1970 and late 1990s. This box also shows 3-6 years signal during the period from 1960-1995. But that signal is not so prominent. Strong annual signals are also found in that box during 1973, 1977, 1982-1983 and 1994. This strong signal of period 1 year is also found in all other boxes during those times. There is a strong 3-7 years signal in box B during 1960s. In box C there are 1-3 year signals in 1964, 1973-1974 and in the late 1990s. In box D also there are 3-8 years signal but significant level is less. The box D is mainly dominated by 1-2 year signals during El-Niño and La-Niña years.

Table 1 show that during the 1991-1992 (one of strong El-Niño years) the remote effect is positive in all boxes except the year 1997-1998 when it is negative. In case of La-Niña years, the negative value is seen in box A. For box B it positive except 1988-1989. For box D, it is negative in 1955-1956, 1973-1974 and positive in 1975-1989. It also shows that when IOD (1988, 1998) occurs concurrently with El-Niño or La-Niña, the boxes shows different type of nature compared to only El-Niño or La-Niña years.

Figure 9 (right column) shows that remote effect is larger in magnitude over climatology in El-Niño event case in the southern BOB and in favor of upwelling. The rest of the BOB is also with positive remote effect except in the central BOB. In IOD year, the remote effect is larger in magnitude than the climatological value in the eastern and the south-eastern sides of BOB. During that year, WSC is very strong for downwelling. Therefore downwelling is still there as it dominates the other effects. Only in the small region of the eastern BOB shows the upwelling. During the La-Niña year, remote effect is prominent and in favor of upwelling in the north-eastern BOB. The favor of downwelling is present all the other regions of the BOB with a stronger in magnitude in the southern coast of Sri Lanka. But during that event the WSC is so strong that the region shows upwelling. Remote effects during the negative IOD events are similar in nature of La-Niña event.

4. Conclusions

Analyzing the SODA data, we have investigated the upwelling and downwelling signals and their variations over BOB basin. The monthly climatology of WSC shows that there is an anti-cyclonic pattern all over the BOB during winter. This anti-cyclonic pattern slowly (May to September) squeezed towards eastern part of the basin. During this time western part of the basin shows another cyclonic pattern. This divides the BOB in two parts as western side with cyclonic WSC and eastern side with anti-cyclonic WSC. During the period from October to December, the BOB again divides in two parts as northern (anti-cyclonic WSC) to southern (cyclonic WSC). The vertical velocity does not corroborate with WSC except summer when the strong southeasterly wind flows over BOB. The remote effect for the BOB is mainly from equatorial region and Malacca channel which is clear from our study. The equatorial remote effect is opposing the wind stress during the summer season but the Malacca Strait influence is in favor of wind stress during the winter time. The northward moving coastal Kelvin waves, penetration of Arabian Sea and Indian Ocean water around 85 E into the BOB basin (Figure 4a) and trapping of Kelvin and Rossby waves in the Central BOB [Yu et al., 1991, Yu 2003; Han and Webstar 2002; . Shankar et al., 1996 and Paul et al., 2009] are the main components of the remote effect (Figure 4b).

In order to gain inside the dynamics of upwelling and downwelling the horizontal advection to the vertical velocity is analyzed which shows that from December to February the warm water advection from the south into the BOB is present when strong downwelling exist. At the same time cold water get advected to the central BOB from eastern coast to the central BOB. With time this cold water advection push back the warm water to the south and occupy most

of the BOB during April. From the month of May when the strong south west wind starts to flow over the BOB, the cold water advection reduces to the west and warm water advection starts to the eastern BOB. In the month of July the warm water advection takes place from the Arabian Sea to the BOB. During the month from September to October again warm water advection starts from the equator to the BOB region.

In the interannual variability, it is seen that curl of wind stress increases after 1980 which in turn results the increase of upwelling in the BOB. The BOB is highly influenced by El-Niño and La-Niña events mostly in the southern part compared to the northern side. There are systematic influences of the boxes by the strong El-Niño and La-Niña events except the period of associated with concurrent IOD event (Table 1). Wavelet analysis for WSC, vertical velocity and remote effect show mainly the prominent yearly and ENSO signal (2 -8 years) indicating the BOB influenced by reversing wind effect and the effect from the ENSO phenomena. The responses of BOB during El- Niño year and during the positive IOD year are similar as well as in the same way La- Niña and negative IOD year are also similar. The explanations for the variations of wind stress curls after 1980 needs detailed investigations using numerical model and that will be our future study.

Acknowledgements
The authors also gratefully acknowledge the financial support given by the Earth System Science Organization (ESSO) – Indian National Centre for Ocean Information Services (INCOIS), Ministry of Earth Sciences, and Government of India to conduct this research.

REFERENCES

1. Carton, J.A., G. Chepurin, and X. Cao (2000a), A Simple Ocean Data Assimilation analysis of the global upper ocean 1950-1995 Part 2: results, *J. Phys. Oceanogr.*, 30, 311–326.
2. Carton, J.A., G. Chepurin, X. Cao, and B.S. Giese (2000b), A Simple Ocean Data Assimilation analysis of the global upper ocean 1950-1995, Part 1: methodology, *J. Phys. Oceanogr.*, 30, 294–309.
3. Carton, J.A., B.S. Giese, and S.A. Grodsky, (2005), Sea level rise and the warming of the oceans in the SODA ocean reanalysis, *J. Geophys. Res.*, 110, art# 10.1029/2004JC002817
4. Chakraborty, A., S. Behera, M. Mujumdar, R. Ohba and T. Yamagata (2006), Diagnosis of Tropospheric Moisture over Saudi Arabia and Influences of IOD and ENSO, *Mon. Wea. Rev*, 134, 598 – 617.
5. Deser, C., M. A. Alexander, and M. S. Timlin (1999), Evidence for a wind-driven intensification of the Kuroshio Current extension from the 1970s to the 1980s, *J. Climate,* 12**,** 1697–1706.
6. Fischer A. S., P. Terray, E. Guilyardy, S. Gualdi., P. Delecluse (2004), Two Independent Triggers for the Indian Ocean Dipole/Zonal Mode in a Coupled GCM, *Journal of Climate,*18,3428-3449
7. Fu, L L (2007), Intraseasonal variability of the equatorial Indian Ocean observed from sea surface height, wind, and temperature data, *J. Phys. Oceanogr*. 37, 188-202.
8. Han, W. and J.P. McCreary (2001), Modeling salinity distribution in the Indian Ocean, *J. Geophys., Res*., 106, 859-877.
9. Han, W., J.P. McCreary, and K.E. Kohler (2001), Influence of P-E and Bay-of-Bengal rivers on dynamics, thermodynamics, and mixed-layer physics in the Indian Ocean, J. Geophys., Res., 106, 6895-6916.
10. Han, W. and P.J. Webster (2002), Forcing Mechanisms of Sea-Level Interannual Variability in the Bay of Bengal, *J. Phys. Oceanogr*., 32, 216-239.
11. Jensen, T. G. (2007), Wind-driven response of the northern Indian Ocean to climate extremes. *J. Climate*, 20, 2978-2993.
12. McCreary, J.P., P.K. Kundu and R.L. Molinari (1993), A numerical investigation of dynamics, thermodynamics and mixed-layer processes in the Indian Ocean, *Prog. in Oceanog.* 31(3), 181–244.
13. McCreary, J.P., W. Han, D. Shankar and S.R. Shetye (1996) , Dynamics of the east India Coastal Current. 2. Numerical solutions, *J. Geophys. Res.,* 101(C6), 13 993–14 000.
14. Paul, S., A. Chakraborty, P. C. Pandey, S. Basu, S. K. Satsangi and M. Ravichandran (2009), Numerical simulation of Bay of Bengal Circulation features from Ocean General Circulation Model, *Marine Geodesy*, 32, 1- 18.
15. Pond, S., and G. Pickard (2005) , Introductory Dynamical Oceanography, Second Edition, New York, *Elsevier Butterworth-Heinemann*, 329 pp.
16. Potemra, J.T., M.E. Luther and J. O'Brien (1991), The seasonal circulation of the upper ocean in the Bay of Bengal, *J. Geophys. Res.,* 96(C7), 12667–12683.
17. Prasad, T. G (1997), Annual and seasonal mean buoyancy fluxes for the tropical Indian Ocean, *Current Science*, 73(8), 667–674.
18. Prasanna Kumar, S., A. S. Unnikrishnan (1995), Seasonal cycle of temperature and associated wave phenomena in the upper layers of the Bay of Bengal, *J. Geophys. Res.,* 100, 13585–13593.
19. Rao L.V.G and P. Shree Ram (2005) , Upper ocean physical process in the tropical Indian ocean; Monogram, NIO, Regional Centre, Vishakhapatnam, 68pp.
20. Rao S.A., S. K. Behera(2005), Subsurface influence on SST in the tropical Indian Ocean: structure and interannual variability, *J. Dyn. Atm. Ocean*, 30, 103-135.
21. Saji N.H., B.N. Goswami, P.N. Vinayachandran, T.Yamagata (1999), A dipole mode in the tropical Indian Ocean, *Nature*, **401**, 360-363.
22. Shankar, D., J. P. McCreary, W. Han and S. R. Shetye (1996) , Dynamics of the East India Coastal Current. 1. Analytic solutions forced by interior Ekman pumping and local alongshore winds. *J. Geophys, Res.,* 101(C6), 13 975–13 991.
23. Shetye, S. R., A. Gouveia, D. Shankar, S. Shenoi, P. Vinayachandran, D. Sundar, G. Michael, and G. Nampoothiri (1996), Hydrography and circulation in the western Bay of Bengal during the Northeast monsoon, *J. Geophys. Res.*, 101, 114011–14025.
24. Shetye, S.R., A.D. Gouvela, S.S.C. Shenoi, D. Sundar, G.S. Michael and G. Nampoothiri (1993), The western boundary current of the seasonal subtropical gyre in the Bay of Bengal, *J. Geophys. Res.,* 98(C1): 945–954.
25. Shetye, S.R., S.S.C. Shenoi, A.D. Gouvela, G.S. Michael, D. Sundar and G. Nampoothiri (1991) , Wind-driven coastal upwelling along the western boundary of the Bay of Bengal during the southwest monsoon, *Continental Shelf Res.,* 11**,** 1397–1408.
26. Somayajulu Y.K., V.S.N. Murty, Y.V.B. Sarma (2003), Seasonal and inter-annual Variability of surface circulation in the Bay of Bengal from TOPEX/Poseidon altimetry, *Deep-Sea Research II*, 50, 867–880.
27. Subramanian V. (1993), Sediment load of Indian rivers, *Current Science*, 64, 928–930.

28. Suryanarayana A., V. S. N. Murty and D. P. Rao (1993), Hydrography and circulation of the Bay of Bengal during early winter, 1983, *Deep-Sea Research I,* 40(1), 205–217.

29. Torrence C. and G. P. Compo (1998), A practcal guide to wavelet analysis. *Bull. Amer. Meteor. Soc.,*79, 61-78

30. Yu, L. (2003), Variability of the depth of the 20˚C isotherm along 6 N in the Bay of Bengal: Its response to remote and local forcing and its relation to satellite SSH variability, *Deep Sea. Res. II.*, 50, 2285-2304.

31. Yu, L., J.J. O'Brien and J.Yang (1991), On the remote forcing to the circulations in the Bay of Bengal. *J. Geophys. Res.,* 96, 20,449-20,454.

Figure captions

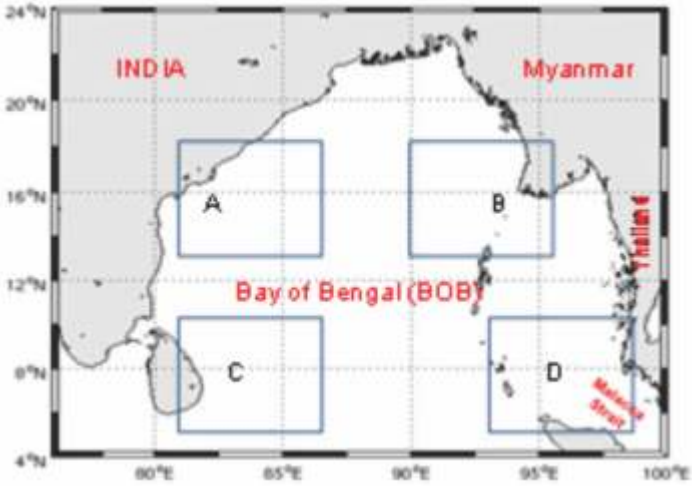

Figure 1: Domain of the study

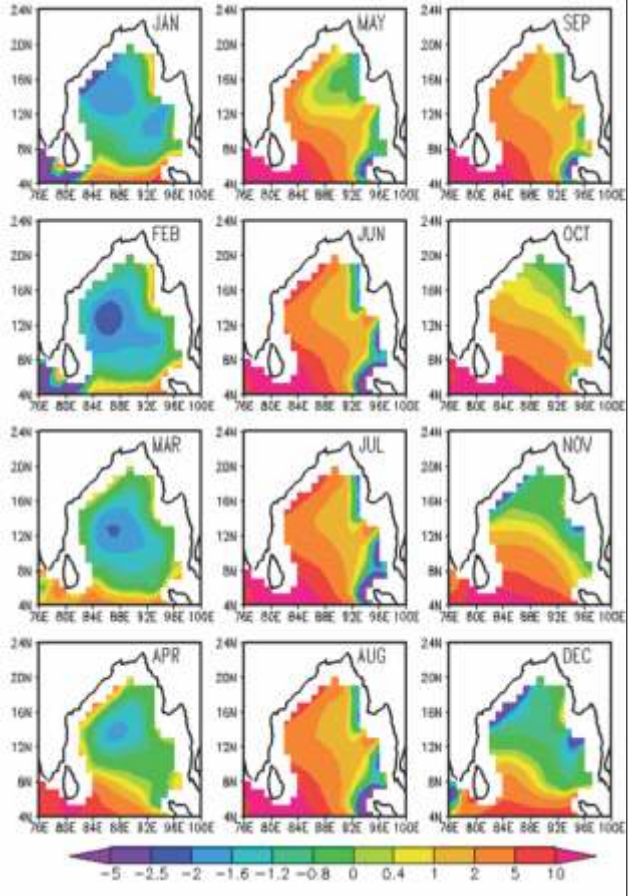

Figure 2: Monthly climatology of wind stress curl (1 Unit = 10^{-6} ms^{-1}).

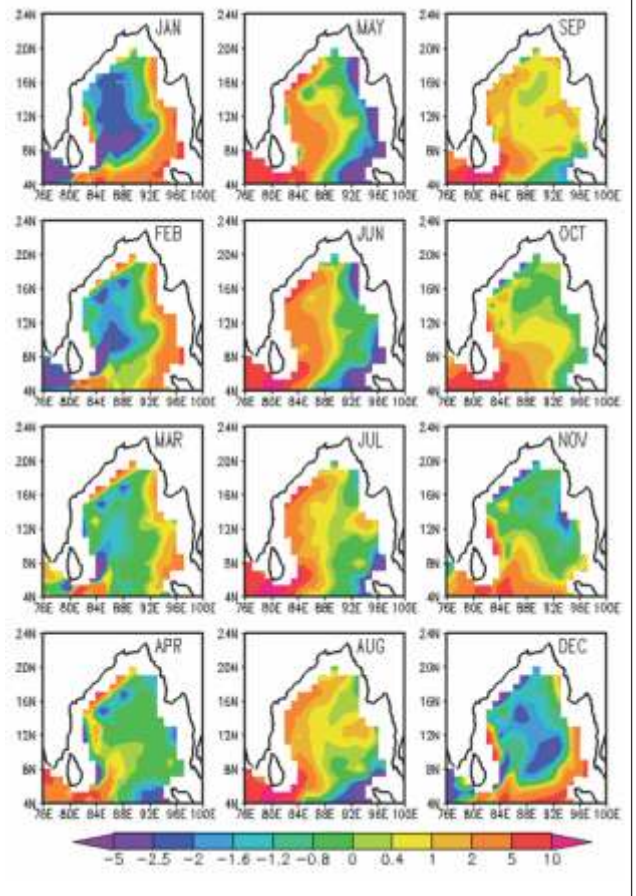

Figure 3: Monthly climatology of vertical velocity (1 Unit = 10^{-6} ms^{-1}).

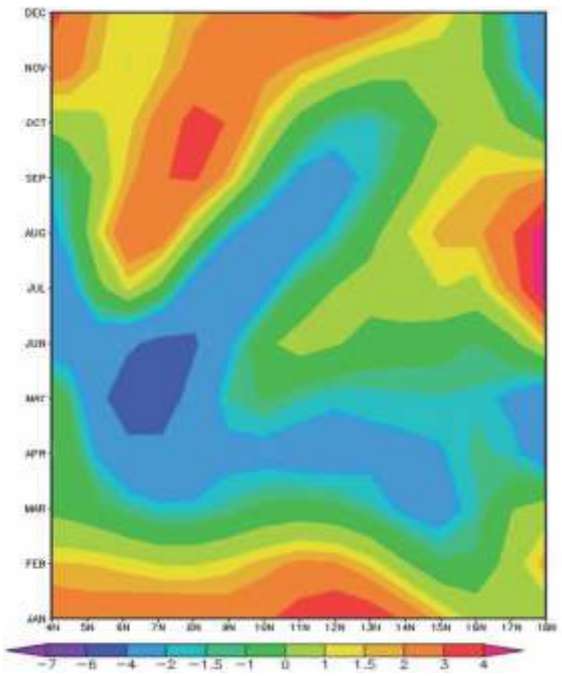

Figure 4a

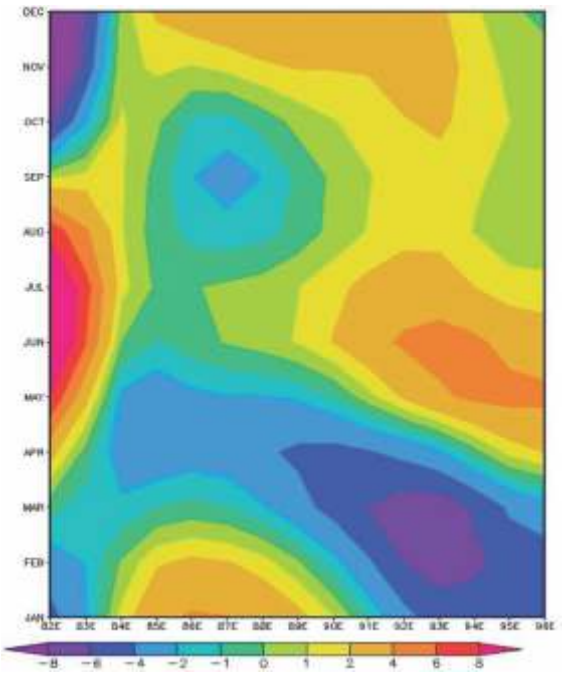

Figure 4b

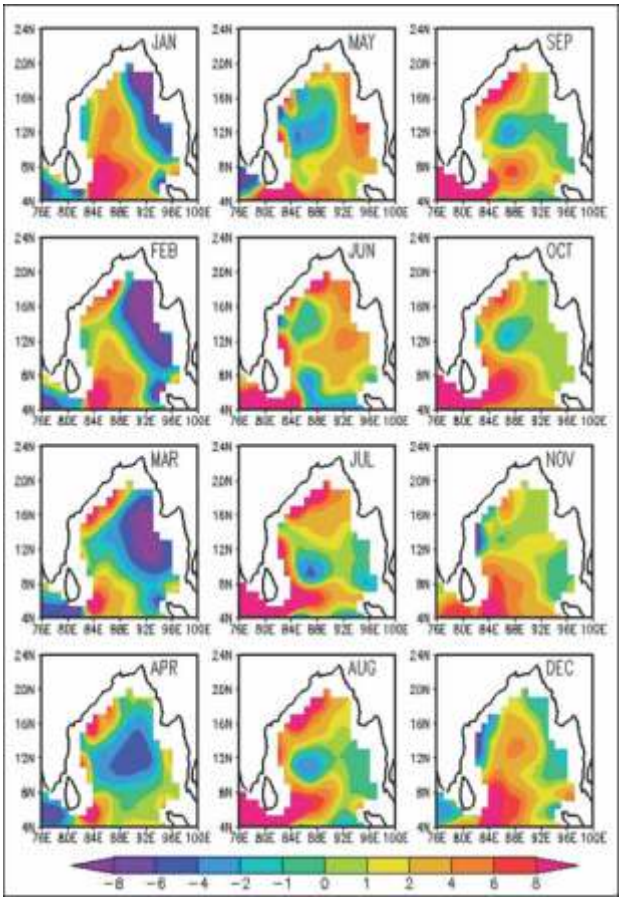

Figure 4c

Figure 4: Monthly variation of temperature advection (1 Unit = 10^{-8} Ks^{-1}) for a) time-latitude section along 85°E, b) time-longitude along 12°N and c) climatology.

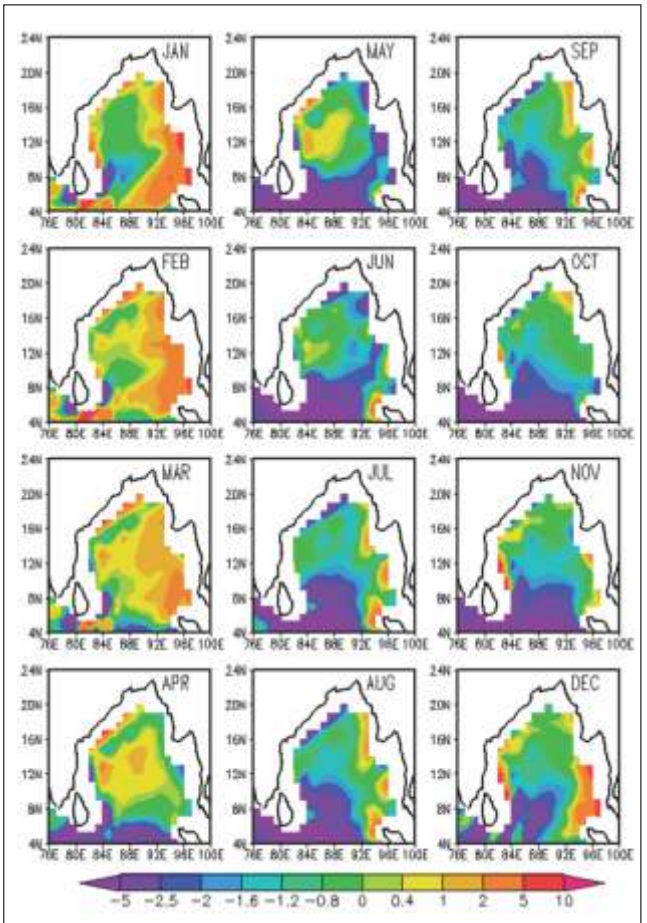

Figure 5: Monthly climatology of remote effect (1 Unit = 10^{-6} ms^{-1}).

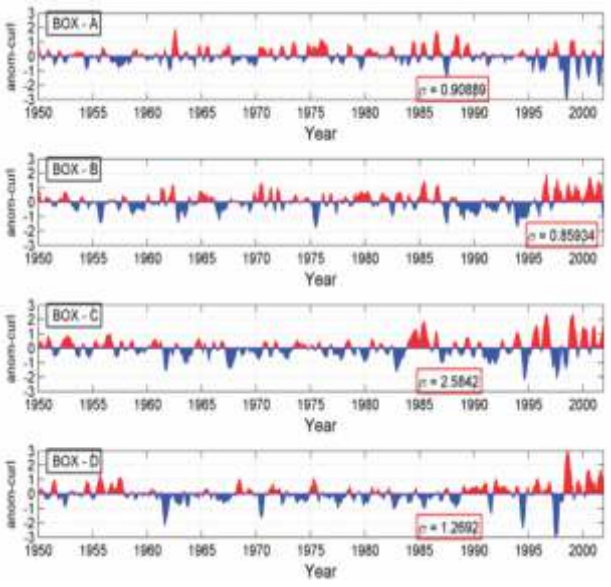

Figure 6a: Interannual variations of wind stress curl indices.

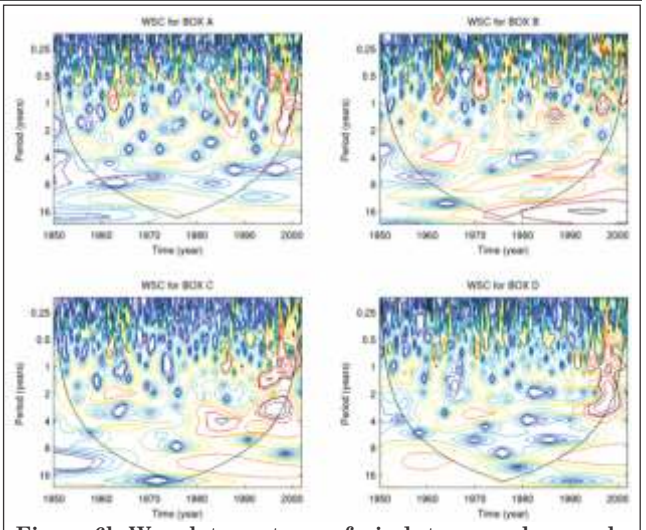

Figure 6b: Wavelet spectrum of wind stress curl anomaly using 'Morlet' wavelet. The thick contour encloses regions of greater than 90% confidence for a red-noise process. Cross-hatched regions on either end indicate the "cone of influence," where edge effects become important.

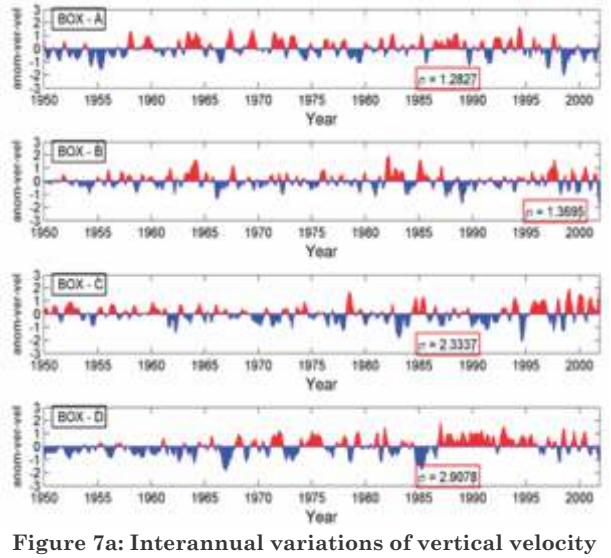

Figure 7a: Interannual variations of vertical velocity indices.

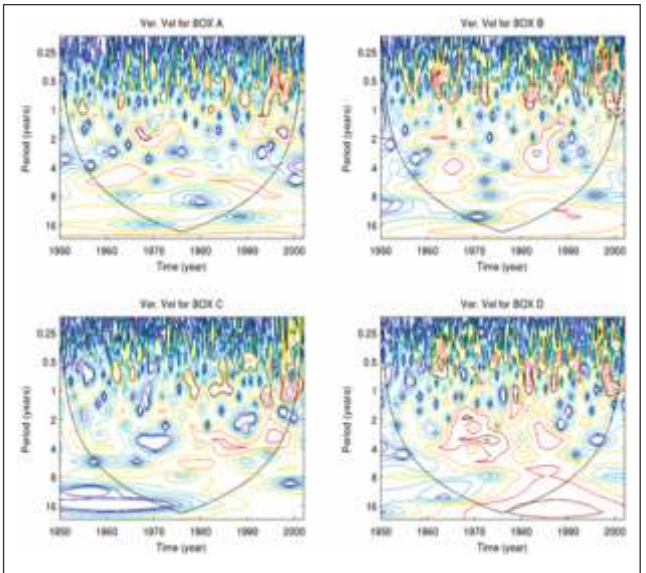

Figure 7b: Same as 6b, but for vertical velocity.

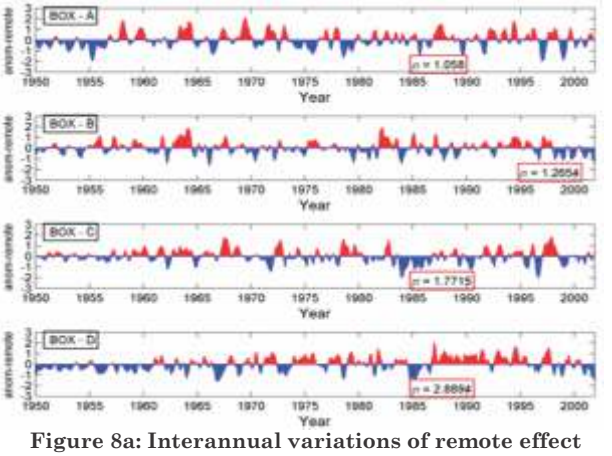

Figure 8a: Interannual variations of remote effect indices.

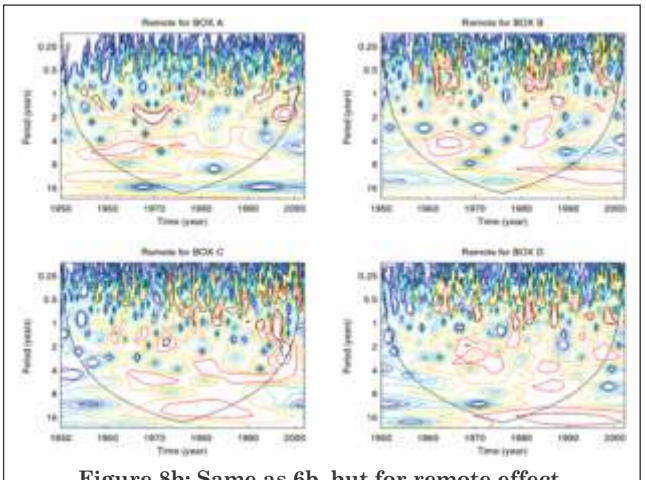

Figure 8b: Same as 6b, but for remote effect.

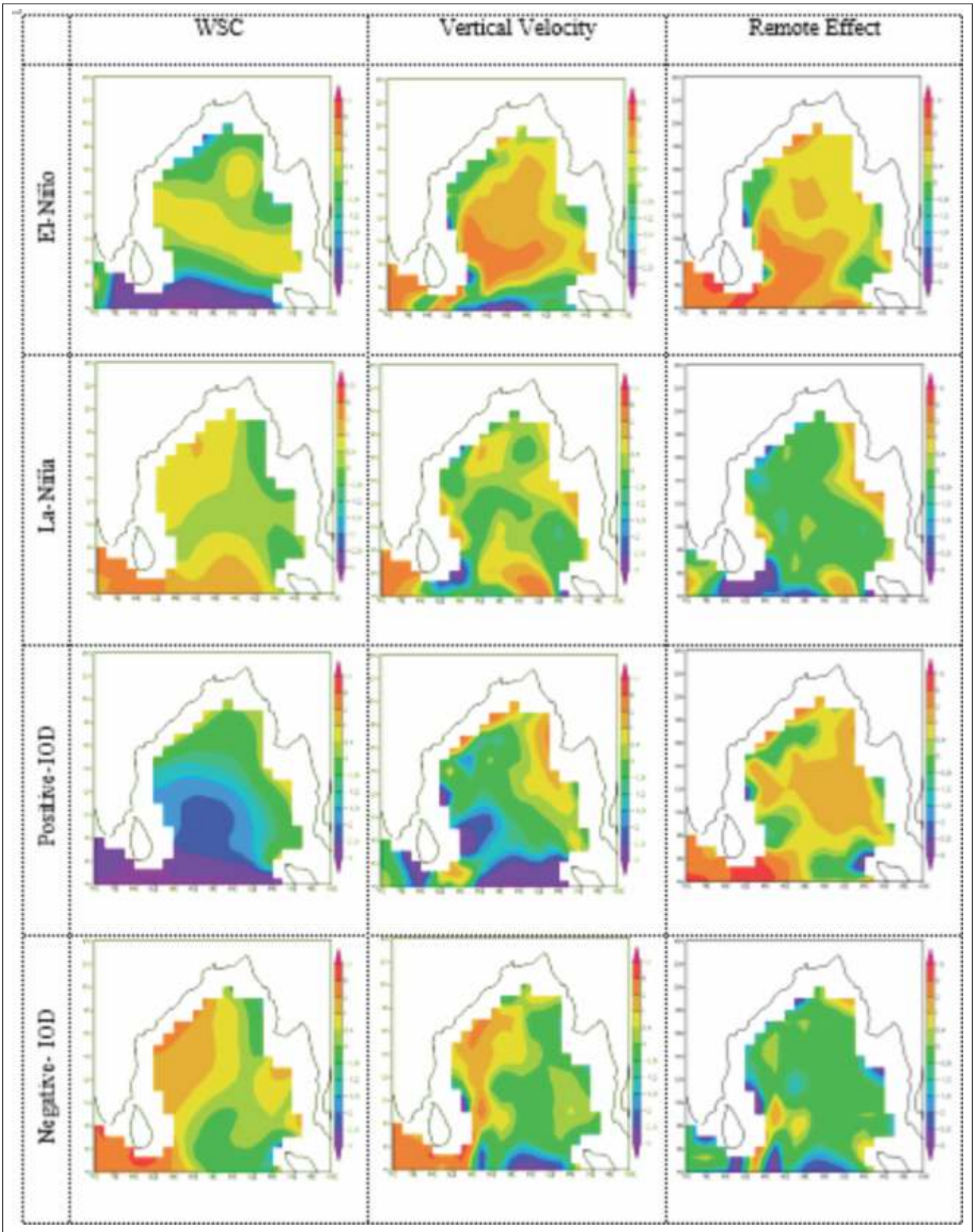

Figure 9: Composite picture of WSC, vertical velocity and remote effect anomalies during strong El-Niño, La-Niña, positive IOD and negative IOD years.

Table 1: Nature of WSC, vertical velocity and remote effect during strong El-Niño and La-Niña years.

Strong El-Niño

Year	WSC (w_E)				Ver-Vel (w_{ver})				Remote Effect (w_{remote})			
	A	B	C	D	A	B	C	D	A	B	C	D
1972-73	0	0	N	N	P	P	N	N	P	P	N	N
1982-83	0	0	N	N	P	P	N	N	P	P	N	N
1991-92	0	0	N	N	P	P	N	N	P	P	P	P
*1997-98	P	P	N	N	0	P	P	0	N	N	N	N

Strong La-Niña

Year	WSC (w_E)				Ver-Vel (w_{ver})				Remote Effect (w_{remote})			
	A	B	C	D	A	B	C	D	A	B	C	D
1955-56	0	0	P	P	N	P	P	0	N	P	N	N
1973-74	0	0	0	0	N	0	P	P	N	0	P	N
1975-76	P	N	0	P	N	N	0	P	N	P	0	P
*1988-89	P	N	P	P	P	0	0	P	0	N	N	P

P → positive, N→ Negative

*indicates the year with IOD.